Elliot Lu, Connor Glosser, Carlo Piermarocchi, and B. Shanker

# Numerical Simulations of Laser Pulse Propagation in Quantum Active Media

## *Using a semiclassical model.*

xxxxx

Active media are materials that consist of quantum systems, such as atoms, impurities, or quantum dots, and are characterized by strong resonant absorption and re-emission of radiation. In this article, we present a general framework for the numerical simulation and analysis of time-dependent radiation-induced phenomena in active media. The formulation used is based on the solution of semiclassical Maxwell–Bloch equations describing the evolution of each quantum element under the effect of external and re-emitted radiation. Within these Maxwell–Bloch equations, the coupling of quantum systems to classical Maxwellian fields poses computational challenges due to the strong nonlinearities involved. In contrast to traditional mesh-based solvers, we adopt an electric field integral-operator approach that can reliably account for near-field effects—including self-radiation—and is scalable to large systems. We then focus on media based on large numbers of quantum dots and demonstrate various physical effects arising from the near-field coupling, including polarization modulations and superradiance.

*Digital Object Identifier 10.1109/MAP.2021.3073147*
*Date of current version: 12 May 2021*

## INTRODUCTION

In contrast to conventional matter that scatters light directly, the term active media refers to matter that modifies propagating waves by absorbing and re-emitting radiation. Such media consist of nanoscale elements, typically atoms and semiconductor quantum dots, characterized by strong optical resonances. These materials see applications as diverse as gain media for lasers, optical amplifiers, and components for quantum technologies. In this respect, quantum dots have a salient advantage over their atomic counterparts. Their stronger dipolar transitions result in more pronounced coupling via secondary radiated (re-emitted) fields and permit the observation of nonlinear effects, such as Rabi oscillations [1]–[3], at lower laser intensities.

The consequences of secondary radiation in quantum dots have been studied extensively in both experimental [4] and theoretical/computational [5], [6] works. In the latter, Maxwell-Bloch equations [7] are typically used to describe the interactions among an ensemble of dots, each modeled as a many-level quantum system. Such a description may be semiclassical, wherein the dots absorb and re-emit classical Maxwellian fields, or the fields may be fully quantized. Regardless, the innate coupling of quantum mechanics to electrodynamics results in a set of equations

that are highly nonlinear and formidable to solve. Theoretical calculations are thus limited to systems with very small numbers (< 10) of emitters and neglect the effects due to the quantization of the electromagnetic fields. Numerical solutions, on the other hand, have witnessed an evolution from continuum models [8], [9] to models employing spatial homogeneity [10] and mesh-based partial differential equation solvers [11], [12].

Major shortcomings of the aforementioned methods are that they are unable to resolve short-ranged effects or scale to larger systems while remaining computationally feasible. In what follows, we present a computational approach to the Maxwell–Bloch equations employing a semiclassical evaluation of time-domain radiated electric fields. Techniques to efficiently and rapidly evaluate these radiated fields are well known [13]–[17] and have been applied to simulations of large numbers of quantum dots. Our contributions are slightly different. While simulation in itself is somewhat compelling, here we focus on the interesting physical effects induced by such couplings, such as oscillatory patterns, polarization modulations, and superradiant emissions [10], [18]. As a result, our contribution in this article is to elucidate the modeling of some of these different physical effects.

## SEMICLASSICAL FORMULATION

In the following, we elucidate a self-consistent model of quantum dot ensembles as well as provide insight into the physics of the model. Each quantum dot can be modeled as a two-level quantum system. Coupling with incident light stimulates the dot from the ground to the excited state and generates a coherent polarization, which, in turn, induces the re-emission of secondary radiation. Such a model sufficiently captures the physics of interactions among dots and fields while being simple enough to admit a readily visualized geometric interpretation.

The Bloch formulation provides this interpretation, wherein the quantum state of each dot is represented in three dimensions, residing (in the absence of decoherence) on the surface of a unit Bloch sphere (Figure 1). A 3D Bloch vector, $\mathbf{s} = (u, v, w)^T$, describes the quantum state of each dot on this sphere. As the south and north "poles" represent the ground and excited states, respectively, the population inversion parameter $w$ is a measure of the "excitedness" of the dot.

An equivalent formulation in terms of a $2 \times 2$ density matrix $\hat{\rho}$ is given by the one-to-one correspondence

$$\rho = \begin{pmatrix} \rho_{00} & \rho_{01} \\ \rho_{10} & \rho_{11} \end{pmatrix} = \frac{1}{2} \begin{pmatrix} 1-w & u+iv \\ u-iv & 1+w \end{pmatrix}. \tag{1}$$

Both here and in what follows, $i$ denotes the imaginary unit.

In the $\rho$ basis, the Liouville equation of motion for each dot (from which the Maxwell–Bloch equations may be derived) is given by

$$\frac{\mathrm{d}\rho}{\mathrm{d}t} = \frac{-i}{\hbar}[\mathcal{H}(t), \rho] - \mathcal{D}[\rho]. \tag{2}$$

Here, the dot Hamiltonian,

$$\mathcal{H}(t) \equiv \begin{pmatrix} 0 & \hbar\chi(t) \\ \hbar\chi^*(t) & \hbar\omega_0 \end{pmatrix}, \tag{3}$$

governs the interaction of the density matrix elements with an electric field $\mathbf{E}(\mathbf{r}, t)$. It consists of diagonal terms representing the internal energies (energy eigenvalues) of each state—$\omega_0$ is the transition frequency proportional to the energy of the excited state—and off-diagonal terms containing the interaction with fields via $\chi(t) = \mathbf{d} \cdot \mathbf{E}(\mathbf{r}, t)/\hbar$. Here, $\mathbf{d}$ is the dipole moment associated with the transition between states that determines the strength and direction of the induced polarization. Additionally, one typically uses a decoherence matrix,

$$\mathcal{D}[\rho] \equiv \begin{pmatrix} (\rho_{00}-1)/T_1 & \rho_{01}/T_2 \\ \rho_{10}/T_2 & \rho_{11}/T_1 \end{pmatrix}, \tag{4}$$

to describe the effects of spontaneous emission on each dot.

The Liouville equation of motion (2) has a physical interpretation in terms of Bloch vectors. Using (1) and assuming real fields, rewriting (2) in terms of Bloch components yields

$$\begin{cases} \dot{u} = -\omega_0 v - u/T_2 \\ \dot{v} = \omega_0 u - 2\chi w - v/T_2 \\ \dot{w} = 2\chi v - (w+1)/T_1 \end{cases}. \tag{5}$$

Disregarding the damping terms, this can be written as a precession equation

$$\dot{\mathbf{s}} = \boldsymbol{\Omega} \times \mathbf{s}, \tag{6}$$

where the effective torque $\boldsymbol{\Omega} = (2\chi, 0, \omega_0)^T$ acts as the axis of rotation of the Bloch vector $\mathbf{s}$. In the absence of electric fields ($\chi = 0$), $\boldsymbol{\Omega}$ is parallel to the $w$-axis, and the system rotates in a plane of constant $w$; thus, there are no transitions between states. The presence of fields tilts $\boldsymbol{\Omega}$ away from the $w$-axis, stimulating transitions (Figure 2). These oscillate between the two states at a rate equal to the Rabi frequency $\chi$, hence the term *Rabi oscillations*.

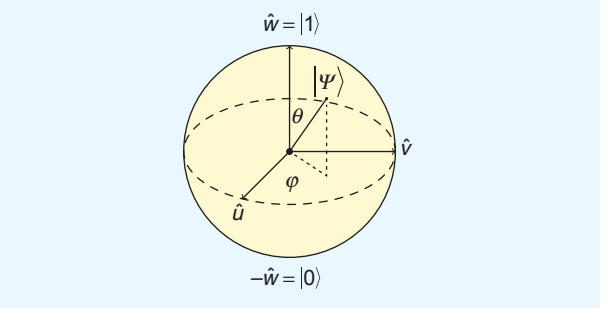


**FIGURE 1.** A Bloch sphere representation of a two-level quantum system. The evolution of $|\psi\rangle$ on the surface of this unit sphere is described by (2). The "poles" $|0\rangle$ and $|1\rangle$ represent the ground and excited levels, respectively [19].

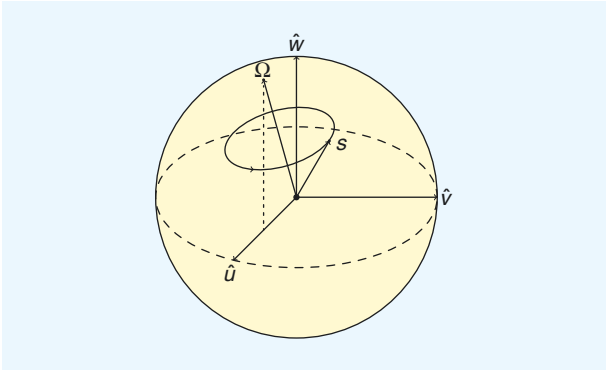


**FIGURE 2.** The precession of a Bloch vector **s** about a torque $\mathbf{\Omega}$ lying in the *uw*-plane. The presence of field excitations tilts $\mathbf{\Omega}$ away from the *w*-axis, causing the *w* component of **s** to depart from its initial value and inducing a transition between states.

### THE ROTATING FRAME AND ROTATING WAVE APPROXIMATION

Consider the simplest system, a single quantum dot excited by an incident laser field $\mathbf{E}_L(\mathbf{r},t)$ oscillating at frequency $\omega_L$, assuming no self-radiation (see the "Self-Radiative Fields" section). In all of the relevant scenarios, this laser is nearly resonant with the transition frequency $\omega_0 \sim \omega_L$ which lies in the optical frequency band ($\sim 2,278\ \mathrm{ps}^{-1}$). Resolving such fast oscillations requires the choice of a very small time step; hence, integrating (2) directly on the timescale of typical Rabi dynamics (~1 ps) becomes computationally laborious. We, therefore, introduce $\tilde{\rho} = U\rho U^{\dagger}$, where $U = \mathrm{diag}(1, e^{i\omega_L t})$ and $U^{\dagger}$ denotes the conjugate transpose of $U$, transforming to a frame rotating with the frequency of the incident laser. In this rotating frame, (2) becomes

$$\frac{\mathrm{d}\tilde{\rho}}{\mathrm{d}t} = \frac{-i}{\hbar}[\tilde{\mathcal{H}}(t), \tilde{\rho}] - \mathcal{D}[\tilde{\rho}], \tag{7}$$

where the rotating frame Hamiltonian,

$$\tilde{H}(t) = \begin{pmatrix} 0 & \hbar\chi(t)e^{-i\omega_L t} \\ \hbar\chi^{*}(t)e^{i\omega_L t} & \hbar(\omega_0 - \omega_L) \end{pmatrix}, \tag{8}$$

contains only terms proportional to $e^{i(\omega_0 \pm \omega_L)t}$ if $\mathbf{E}_L(t) \sim \tilde{\mathbf{E}}_L(t)\cos(\omega_L t)$. We neglect the high frequencies $\omega_0 + \omega_L$, assuming that terms containing them will integrate to zero in solving (7) over appreciable timescales—an approximation known as the rotating wave approximation (RWA).

Thus, only terms containing the downshifted frequency $\omega_0 - \omega_L$ remain, effecting a drastic reduction in the number of time steps required to solve (7). In terms of Bloch vectors, the rotating frame equivalent of (5) is

$$\begin{cases} \dot{\tilde{u}} = (\omega_L - \omega_0)\tilde{v} - 2\chi\sin(\omega_L t)\tilde{w} - \tilde{u}/T_2 \\ \dot{\tilde{v}} = -(\omega_L - \omega_0)\tilde{u} - 2\chi\cos(\omega_L t)\tilde{w} - \tilde{v}/T_2 \\ \dot{\tilde{w}} = 2\chi(\tilde{v}\cos(\omega_L t) + \tilde{u}\sin(\omega_L t)) - (\tilde{w}+1)/T_1 \end{cases}, \tag{9}$$

which obeys the same precession as (6) but with the effective torque $\tilde{\mathbf{\Omega}} = (2\chi\cos(\omega_L t), -2\chi\cos(\omega_L t), \omega_0 - \omega_L)^T$ As the Bloch vector is now rotating with the frequency of the excitation $\omega_L$, $\tilde{\mathbf{\Omega}}$ is effectively downshifted along the *w*-axis. Nonetheless, its components transverse to the *w*-axis are still oscillating at the fast frequency $\omega_L$.

By writing $\chi = \tilde{\chi}\cos(\omega_L t) = (\mathbf{d}\cdot\tilde{\mathbf{E}}(\mathbf{r},t)/\hbar)\cos(\omega_L t)$, one can readily show that (9) under the RWA simplifies to

$$\begin{cases} \dot{\tilde{u}} = (\omega_L - \omega_0)\tilde{v} - \tilde{u}/T_2 \\ \dot{\tilde{v}} = -(\omega_L - \omega_0)\tilde{u} - 2\tilde{\chi}\tilde{w} - \tilde{v}/T_2 \\ \dot{\tilde{w}} = 2\tilde{\chi}\tilde{v} - (\tilde{w}+1)/T_1 \end{cases}. \tag{10}$$

The effective RWA torque $\tilde{\mathbf{\Omega}} = (2\tilde{\chi}, 0, \omega_0 - \omega_L)^T$ now contains only slowly varying terms, simplifying the analysis. Further assuming the resonance condition $\omega_L = \omega_0$ and ignoring damping terms, (10) admits the solution [20]

$$\begin{cases} \tilde{u} = \tilde{u}_0 \\ \tilde{v} = -\tilde{w}_0\sin\theta(t) + \tilde{v}_0\cos\theta(t) \\ \tilde{w} = \tilde{v}_0\sin\theta(t) + \tilde{w}_0\cos\theta(t) \end{cases}. \tag{11}$$

The Bloch vector now precesses in a plane of constant $\tilde{u}$, and $\theta(t) = \int_{-\infty}^{t} 2\tilde{\chi}(t')dt'$ gives the angle by which it is rotated in this plane from its initial position $(\tilde{u}_0, \tilde{v}_0, \tilde{w}_0)^T$. For instance, if the Bloch vector starts in the ground state $(0,0,-1)^T$, an angle $\theta(t) = \pi$ will tip it to the excited state $(0,0,1)^T$ in time $t$, and hence we get the term $\pi$ pulse (or, in general, $\theta$ pulse). In the "Consequences of Interdot Coupling" section, a Gaussian waveform of appropriate amplitude will be used as a $\pi$ pulse to stimulate the transitions to the excited state.

### RADIATION FIELDS AND INTERDOT COUPLING

When multiple dots are present, their secondary radiated fields are added to the laser field in calculating the total electric field experienced by each dot as

$$\mathbf{E}(\mathbf{r},t) = \mathbf{E}_L(\mathbf{r},t) + \mathfrak{F}\{\mathbf{P}(\mathbf{r},t)\}. \tag{12}$$

Here, we assume that the radiation field $\mathfrak{F}\{\mathbf{P}(\mathbf{r},t)\}$ arises from a polarization density $\mathbf{P}(\mathbf{r},t) = 2\mathbf{d}\,\mathrm{Re}\{\rho_{01}(\mathbf{r},t)\}$. The radiated field can be obtained by convolving the time derivative of the dyadic Green's function with the polarization source as

$$\begin{aligned} \mathfrak{F}\{\mathbf{P}(\mathbf{r},t)\} &\doteq -\mu_0(\partial_t^2\mathrm{I} - c^2\nabla\nabla)g(\mathbf{r},t) \star_{st} \mathbf{P}(\mathbf{r},t) \\ &= \frac{-1}{4\pi\epsilon}\int\left[(\mathrm{I} - \bar{\mathbf{r}}\otimes\bar{\mathbf{r}})\cdot\frac{\partial_t^2\mathbf{P}(\mathbf{r}',t_R)}{c^2R}\right. \\ &\quad \left. + (\mathrm{I} - 3\bar{\mathbf{r}}\otimes\bar{\mathbf{r}})\cdot\left(\frac{\partial_t\mathbf{P}(\mathbf{r}',t_R)}{cR^2} + \frac{\mathbf{P}(\mathbf{r}',t_R)}{R^3}\right)\right]d^3\mathbf{r}'. \end{aligned} \tag{13}$$

Here, $g(\mathbf{r},t) = \delta(t_R)/R$ is the retarded Green's function, $\mathbf{R} = \mathbf{r} - \mathbf{r}'$, $\bar{\mathbf{r}} = \mathbf{R}/R$, $\otimes$ is a tensor product, and $t_R = t - R/c$.

As the polarization density $\mathbf{P}(\mathbf{r},t)$ arises from the off-diagonal elements of $\hat{\rho}$, this formulation effectively couples the evolution of all of the quantum dots via their radiated fields $\mathfrak{F}\{\mathbf{P}(\mathbf{r},t)\}$. Furthermore, it depicts the propagation of electric signals through space with finite velocity such that each dot receives the field radiated by another dot at the retarded time $t_R$.

In the rotating frame, the source distribution transforms as $\mathbf{P}(\mathbf{r},t)=\mathrm{Re}\{\tilde{\mathbf{P}}(\mathbf{r},t)e^{i\omega_L t}\}$. Substitution into (13) gives the rotating frame equivalent of the radiated field.

### SELF-RADIATIVE FIELDS

So far, we have disregarded the possibility of a dot experiencing its own radiated field. This is a reasonable assumption for modeling simple interactions but will be inadequate for describing collective emission effects such as superradiance, where dots are strongly coupled within their near fields.

An expression for the self-radiation field (or radiation reaction field) $\mathbf{E}_{RR}$ may be derived from (13) by Taylor expanding terms in the Fourier representation of the Green's function [21]. In the rotating frame, the result is

$$\mathbf{E}_{RR}(\mathbf{r},t)\equiv\frac{-1}{4\pi\epsilon}\frac{2}{3c^3}\mathrm{Re}\big[\partial_t^3\tilde{\mathbf{P}}(\mathbf{r},t)+i3\omega_L\partial_t^2\tilde{\mathbf{P}}(\mathbf{r},t)-3\omega_L^2\partial_t\tilde{\mathbf{P}}(\mathbf{r},t)-i\omega_L^3\tilde{\mathbf{P}}(\mathbf{r},t)\big]. \tag{14}$$

Assuming that the polarization varies appreciably slower than the laser oscillation, the last term in (14) will dominate. When this term is substituted into (7), the radiation reaction field yields an effective nonlinear damping term to the right-hand side of that equation, giving

$$\dot{\tilde{\rho}}_{RR}\equiv\frac{\beta}{2}\begin{pmatrix}-((1-2\rho_{00})^2-1) & 2\rho_{01}(1-2\rho_{00})\\ 2\rho_{10}(1-2\rho_{00}) & (1-2\rho_{00})^2-1\end{pmatrix}. \tag{15}$$

Here, $\beta=(1/4\pi\epsilon)(2d^2\omega_L^3/3\hbar c^3)$ is a dimensionless parameter characterizing the strength of damping [18]. In contrast to the damping matrix (4), the radiation reaction damping is decidedly nonlinear. As shall be demonstrated in the "Consequences of Interdot Coupling" section, the inclusion of self-radiative fields gives rise to characteristic superradiant curves.

## COMPUTATIONAL APPROACH

Next, we discuss the problem of solving the system of coupled Liouville equations for each of $N_s$ quantum dots using $N_t$ time steps of equal spacing $\Delta t$. These time steps are chosen to accurately sample the dynamics of the physical quantities involved. As the rotating frame affords us a reduction by a factor $\sim\omega_L/\chi$ in the required $N_t$, we will hereafter assume the rotating frame unless otherwise stated.

### SPATIAL AND TEMPORAL DISCRETIZATION

To solve (7), we begin by representing $\tilde{\mathbf{P}}(\mathbf{r},t)$ in terms of space- and time-basis functions such that

$$\tilde{\mathbf{P}}(\mathbf{r},t)\approx\sum_{\ell=0}^{N_s-1}\sum_{m=0}^{N_t-1}\tilde{\mathcal{A}}_\ell^{(m)}\mathbf{s}_\ell(\mathbf{r})T(t-m\Delta t). \tag{16}$$

Assuming that the dots are point sources, we take $\mathbf{s}_l(\mathbf{r})=\mathbf{d}_l\delta(\mathbf{r}-\mathbf{r}_l)$. Here, $\delta(\mathbf{r})$ is a 3D delta function, $\mathbf{d}_l$ and $\mathbf{r}_l$ denote respectively the dipole moment and position of the $\ell$th dot, while $\tilde{\mathcal{A}}_\ell^{(m)}=2\,\mathrm{Re}(\tilde{\rho}_{\ell,01}(m\Delta t))$ represents its polarization at the $m$th time step.

The time basis functions $T(t)$ interpolate the function of interest at each time step and are required to have finite support and obey the causality clause $T(t)=0$ if $t<-\Delta t$. Additionally, they must be at least twice differentiable to recover the time derivatives in (13). To this end, we elect to use shifted, backward-looking Lagrange polynomials (Figure 3) of order $p=3$ or higher [17].

Substituting (16) into (12) via (13) and projecting the result onto the $\delta(t-m\Delta t)\mathbf{s}_\ell(\mathbf{r})$ basis yields a set of discrete convolution equations,

$$\tilde{\mathcal{E}}^{(m)}=\tilde{\mathcal{E}}_{\mathrm{L}}^{(m)}+\sum_{m'=0}^{m}\tilde{\mathcal{F}}^{(m-m')}\cdot\tilde{\mathcal{A}}^{(m')}, \tag{17}$$

where

$$\tilde{\mathcal{E}}_\ell^{(m)}\equiv\langle\mathbf{s}_\ell(\mathbf{r}),\tilde{\mathbf{E}}(\mathbf{r},m\Delta t)\rangle;\quad 0\le\ell<N_s, \tag{18a}$$

$$\tilde{\mathcal{E}}_{\mathrm{L},\ell}^{(m)}\equiv\langle\mathbf{s}_\ell(\mathbf{r}),\tilde{\mathbf{E}}_{\mathrm{L}}(\mathbf{r},m\Delta t)\rangle;\quad 0\le\ell<N_s, \tag{18b}$$

and $\tilde{\mathcal{F}}^{(k)}$ give a sparse matrix of dimension $N_s\times N_s$ such that

$$\tilde{\mathcal{F}}_{\ell\ell'}^{(k)}\equiv\langle\mathbf{s}_\ell(\mathbf{r}),\tilde{\mathfrak{F}}\{\mathbf{s}_{\ell'}(\mathbf{r})T(k\Delta t)\}\rangle. \tag{18c}$$

Note that due to the finite support of the 3D retarded potential, $\tilde{\mathcal{F}}^{(k)}$ has a sparse, Toeplitz lower-triangular structure (see Figure 4). This facilitates a cost complexity of $O(N_t)$, as only a fixed number of multiplications need to be performed at each time step $m\Delta t$ [17].

### INTEGRATION OF EQUATION OF MOTION

A marching-on-time (MoT) scheme is defined in (17) for evaluating the total electric field. The determination of the polarization $\tilde{\mathcal{A}}^{(m+1)}$ thus proceeds from integrating the equation of motion (7) from $t_i=m\Delta t$ to $t_f=(m+1)\Delta t$ for every quantum dot. To solve this system, we use a predictor corrector derived in [22]. Defining $t_m\equiv m\Delta t$ and approximating $\tilde{\rho}(t)$ as a weighted sum of exponentials, the predictor–corrector scheme proceeds with an extrapolation predictor step

$$\tilde{\rho}_\ell(t_{m+1})\leftarrow\sum_{w=0}^{W-1}\mathcal{P}_w^{(0)}\tilde{\rho}_\ell(t_{m-w})+\mathcal{P}_w^{(1)}\partial_t\tilde{\rho}_\ell(t_{m-w}), \tag{20}$$

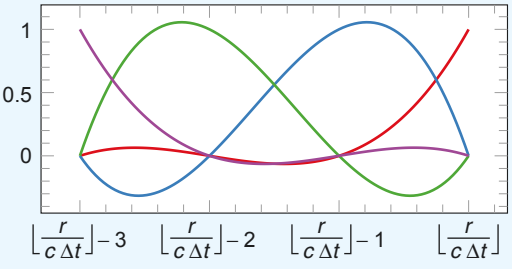


**FIGURE 3.** A set of Lagrange polynomials, serving as time basis functions for the polarization source $\tilde{\mathbf{P}}(\mathbf{r},t)$.

$$\underbrace{\begin{pmatrix}\tilde{\mathcal{E}}^{(0)}\\ \tilde{\mathcal{E}}^{(1)}\\ \tilde{\mathcal{E}}^{(2)}\\ \tilde{\mathcal{E}}^{(3)}\\ \tilde{\mathcal{E}}^{(4)}\end{pmatrix}}_{\text{Total Field}} = \underbrace{\begin{pmatrix}\tilde{\mathcal{E}}^{(0)}_{\text{inc}}\\ \tilde{\mathcal{E}}^{(1)}_{\text{inc}}\\ \tilde{\mathcal{E}}^{(2)}_{\text{inc}}\\ \tilde{\mathcal{E}}^{(3)}_{\text{inc}}\\ \tilde{\mathcal{E}}^{(4)}_{\text{inc}}\end{pmatrix}}_{\text{Laser}} + \underbrace{\underbrace{\begin{pmatrix}\tilde{\mathcal{F}}^{(0)} & & & & \\ \tilde{\mathcal{F}}^{(1)} & \tilde{\mathcal{F}}^{(0)} & & & \\ \tilde{\mathcal{F}}^{(2)} & \tilde{\mathcal{F}}^{(1)} & \tilde{\mathcal{F}}^{(0)} & & \\ & \tilde{\mathcal{F}}^{(2)} & \tilde{\mathcal{F}}^{(1)} & \tilde{\mathcal{F}}^{(0)} & \\ & & \tilde{\mathcal{F}}^{(2)} & \tilde{\mathcal{F}}^{(1)} & \tilde{\mathcal{F}}^{(0)}\end{pmatrix}}_{\text{Precalculated Interaction Weights}} \underbrace{\begin{pmatrix}\tilde{\mathcal{A}}^{(0)}\\ \tilde{\mathcal{A}}^{(1)}\\ \tilde{\mathcal{A}}^{(2)}\\ \tilde{\mathcal{A}}^{(3)}\\ \tilde{\mathcal{A}}^{(4)}\end{pmatrix}}_{\text{Sources}}}_{\text{Radiation Field}} \tag{19}$$

**FIGURE 4.** The matrices of (17) written out explicitly, showing the Toeplitz lower-triangular structure of the convolution matrix.

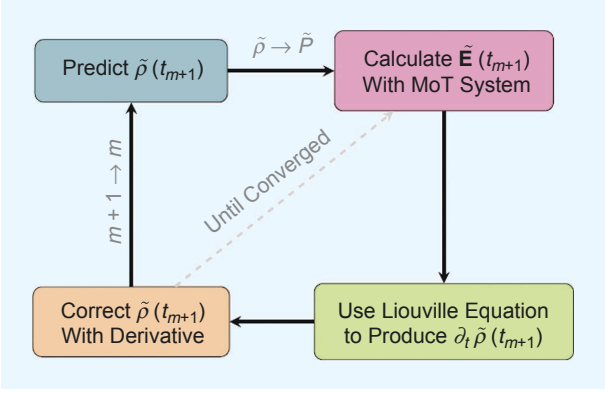


**FIGURE 5.** A flowchart of one iteration of the predictor–corrector for the integration of (7) from $t = m\Delta t$ to $(m+1)\Delta t$.

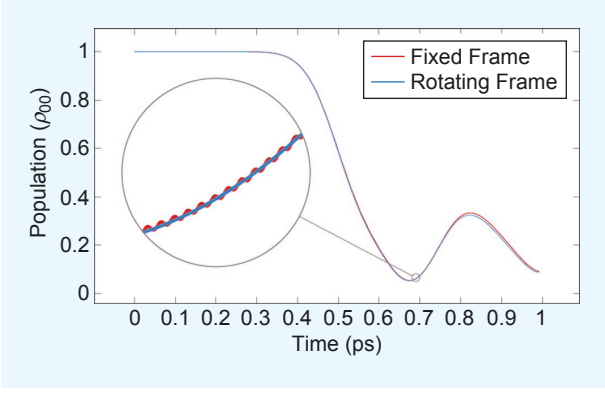


**FIGURE 6.** A comparison of $\rho_{00}(t)$ using both fixed (requiring 59,959 time steps) and rotating (requiring 160 time steps) reference frames for two interacting quantum dots. Both frames produce similar trajectories; however, the inset spy reveals that the fixed frame contains a minute oscillatory term that the rotating frame does not [19].

and iterated corrector steps

$$\tilde{\rho}_\ell(t_{m+1}) \leftarrow \sum_{w=-1}^{W-1} C_w^{(0)}\,\tilde{\rho}_\ell(t_{m-w}) + C_w^{(1)}\,\partial_t \tilde{\rho}_\ell(t_{m-w}). \tag{21}$$

Such an integrator has significantly better convergence properties than Runge–Kutta integrators for equations of the type seen in (7) and naturally accommodates basis functions within $c\Delta t$ of each other. The general iteration procedure for any time step $(m+1)$ is illustrated in Figure 5.

A self-consistent solution to (7) has the following prescription for any time step: 1) determine $\tilde{\mathcal{A}}_\ell^{(m)} = 2\,\mathrm{Re}\,(\tilde{\rho}_{\ell,01}(m\Delta t))$ from the known history of the system, 2) compute $\tilde{\mathcal{E}}_\ell^{(m)}$ using (17), 3) find $\partial_t \tilde{\rho}_{\ell,01}(m\Delta t)$ using (7), and 4) correct $\tilde{\rho}_{\ell,01}(m\Delta t)$ and iterate steps 2–4 until converged [17].

## CONSEQUENCES OF INTERDOT COUPLING

Here we adopt the semiclassical formalism discussed previously to simulate several physical effects that arise from the coupling of dots via their radiated fields—at either long or short distances. In all simulations, we will employ an incident field with the shifted Gaussian waveform

$$\mathbf{E}_{\mathrm{L}}(\mathbf{r}, t) = E_0\, e^{-\frac{(\mathbf{k}\cdot\mathbf{r} - \omega_L(t-t_0))^2}{2\sigma^2}} \cos\omega_L t\, \hat{\mathbf{X}} \tag{22}$$

to excite an ensemble of dots lying initially in the ground state $(\tilde{\rho}_{00}, \tilde{\rho}_{01})|_{t=0} = (1, 0)$, with their density matrix elements evolving according to (7).

Here, $\omega_L = 1{,}500$ meV$/\hbar \approx 2{,}278.9013$ ps$^{-1}$, $\sigma/\omega_L = 1$ ps, $\mathbf{k} = \omega_L/c\,\hat{\mathbf{z}}$, and the laser amplitude $E_0$ is chosen to produce a $\pi$ pulse. The pulse is chosen to peak at $t_0 = 5$ ps, thus exciting the dots at an early time and allowing for the subsequent re-emission of radiation to occur.

To demonstrate the equivalence of the fixed and rotating frames described in the "Semiclassical Formulation" section, a simulation was first performed with two interacting dots. Figure 6 illustrates that the two frames agree up to minute oscillations in the fixed frame about the rotating frame.

### *LONG-RANGE EFFECTS*

We now exhibit some effects of coupling in systems with interdot distances ranging from short to comparable to or greater than the excitation wavelength ($\lambda \approx 827$ nm). As the goal is to study the long-range effects, no self-radiation fields are included here.

In the first simulation, 10,000 quantum dots are randomly distributed in a cylinder of radius 0.2 μm and length 4 μm. Each dot has an identical (fixed) dipole moment $\mathbf{d} = 10\,e\,a_0\hat{\mathbf{x}}$, where $a_0$ is the Bohr radius. While this implies an average interdot distance much smaller than the wavelength, interactions among those dots that are well separated within the cylinder give rise to long-range effects.

Figure 7 shows the polarization of each dot in the cylinder as a function of their **z**-coordinate (the axis of the cylinder) under the effect of a resonant $\pi$ pulse. Evident is the oscillation of the polarization due to the long-range collective effects. This reflects the role of boundary conditions in the confinement of the macroscopic electric field in the system. Additionally, note how the secondary radiation produces random shifts in the polarization due to the short-range effects in the local neighborhood of each dot.

A second simulation was performed involving a larger system of 100,000 dots randomly distributed in a rectangular cuboid of width $\approx 529$ nm and length $\approx 49.59$ $\mu$m. In this simulation,

the dipole moment of each dot has fixed magnitude $|\mathbf{d}| = 10\, e\, a_0$ but a random orientation. Figure 8 displays a color map of $|\tilde{\rho}_{01}|$ as an indicator of the polarization $|\tilde{\mathbf{P}}|$ of each dot at different time steps after the pulse peak. The figure shows only those dots located in a central segment of about 4 μm of the entire cuboid. The random orientation of the dipole moments creates a variation in the amplitude of the polarization with dots whose dipole moments (anti) align with the laser field having the greatest amplitude—hence the multihued appearance of the plots.

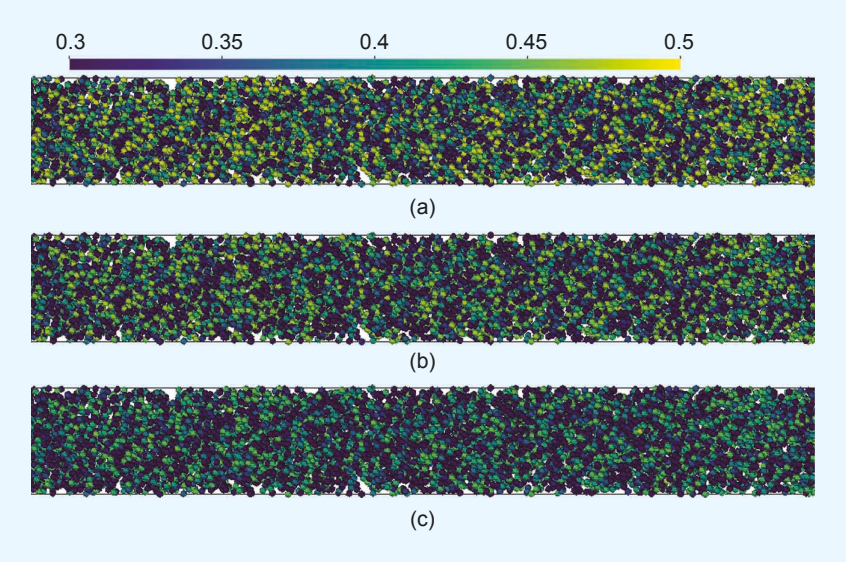


**FIGURE 8.** The coloration of $|\tilde{\rho}_{01}|$ as an indicator of $|\tilde{\mathbf{P}}|$ at (a) $t_1 = 6$ ps, (b) $t_2 = 7$ ps, and (c) $t_3 = 8$ ps, relative to the peak of a 1-ps-wide pulse for a system of 100,000 dots [17].

## SHORT-RANGE EFFECTS AND SUPERRADIANT EMISSIONS

In the following simulation, we include the self-radiation field at the location of each dot. As the overall magnitude of this field is small ($\beta \approx 1.79 \times 10^{-4}$), the simulation must be run at a timescale of $T = 10{,}000$ ps to faithfully observe the long-term effects of the resulting coupling. As the time complexity scales as $O(N_t)$, this limits the number of dots $N$ that can be efficiently simulated. Here we restrict ourselves to a system of, at most, 120 dots randomly placed within a cube of side length $0.100\,\lambda$, thus enabling denser configurations and more intense coupling with increasing $N$. To mitigate the variations due to the random distribution of a comparably small number of dots, multiple trials are taken and the results averaged. Finally, we neglect the linear damping matrix (4) under the assumption that the radiation reaction fields provide the necessary damping via (15).

Figure 9 illustrates the effects of radiation reaction damping on both the population inversion $w$ (the proportion of excited states) and the magnitude of polarization (proportional to the amplitude of the radiated field). We observe with increasing $N$ an increase in the rate of initial decay from excited states and a leftward shift in the peak of polarization. The time behavior of the population inversion was fit with a decaying hyperbolic

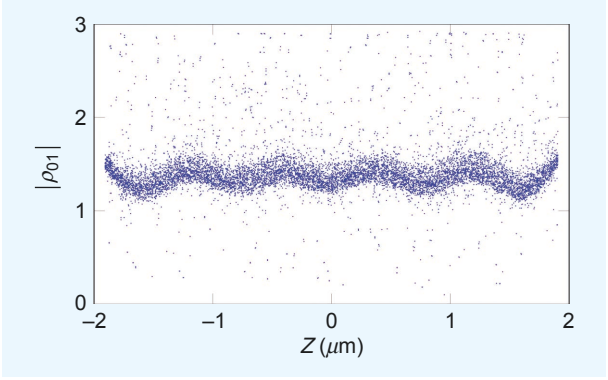


**FIGURE 7.** The $\hat{\mathbf{z}}$-distribution of polarization $|\tilde{\rho}_{01}|$ for a 10,000 dot cylindrical simulation [17].

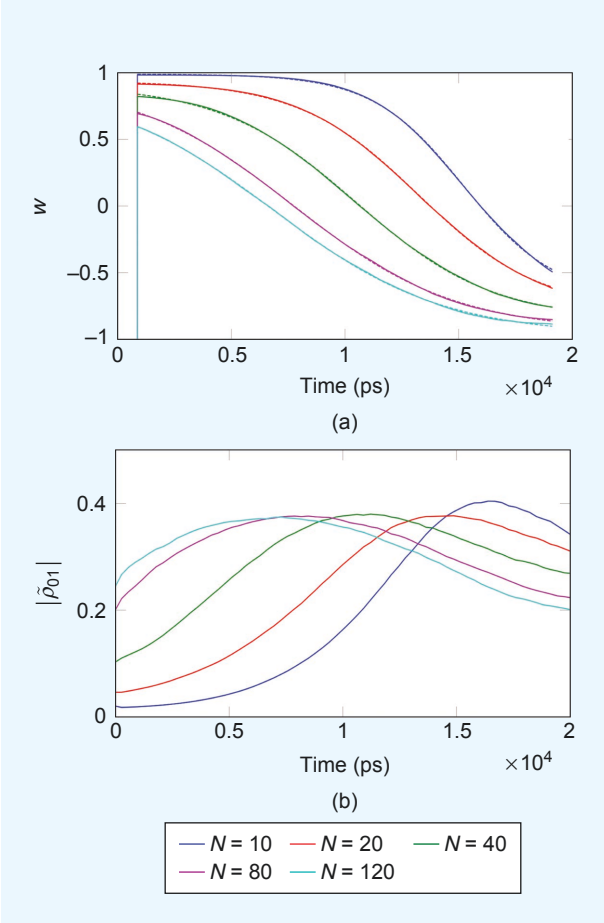


**FIGURE 9.** The (a) population inversion $w$ and (b) magnitude of polarization $|\tilde{\rho}_{01}|$ averaged over all dots, for $N = 10/20/40/80/120$. In the population inversion, the curves of best fit (dashed) for a decaying hyperbolic tangent are shown; the initial rise is due to the incidence of the laser excitation.

tangent that describes the average energy of a two-level system subjected to radiation reaction damping [10]. Both trends are characteristic of superradiance and consistent with previous studies [23], [24].

## CONCLUSIONS

We have shown that a semiclassical model that combines quantum two-level systems and integral-operator-based electric fields can adequately model both long- and short-range radiative coupling effects in active media such as quantum dots. In regimes where the separation between dots is comparable to or greater than the excitation wavelength, oscillatory patterns and polarization modulations are observed. When the dots are separated by smaller distances, the inclusion of self-radiative fields induces superradiant emissions. These are exemplified by changes in the time behavior of the population inversion and polarization, depending on the number of dots participating in the collective effect.

In this article, these were illustrated using a small number of dots. Extending this to a larger number of dots implies integrating the ideas presented here into a more computationally efficient scheme [17] to reduce the spatial complexity as well as using extrapolation methods [25], [26] to reduce the number of required time steps.

## ACKNOWLEDGMENTS

We gratefully acknowledge the High-Performance Computing Center facility at Michigan State University for its support of this work. We also acknowledge support from the National Science Foundation under OAC-1835267.

## AUTHOR INFORMATION

***Elliot Lu*** (luelliot@msu.edu) is with the Department of Physics and Astronomy, Michigan State University, East Lansing, Michigan, 48823, USA.

***Connor Glosser*** (glosser1@msu.edu) is with the Department of Physics and Astronomy, Michigan State University, East Lansing, Michigan, 48823, USA.

***Carlo Piermarocchi*** (piermaro@msu.edu) is with the Department of Physics and Astronomy, Michigan State University, East Lansing, Michigan, 48823, USA.

***B. Shanker*** (bshanker@egr.msu.edu) is with the Department of Physics and Astronomy, Michigan State University, East Lansing, Michigan, 48823, USA. He is a Fellow of IEEE.

## REFERENCES

[1] T. H. Stievater et al., "Rabi oscillations of excitons in single quantum dots," *Phys. Rev. Lett.*, vol. 87, no. 13, p. 133,603, Sept. 2001. doi: 10.1103/PhysRevLett.87.133603.

[2] H. Kamada, H. Gotoh, J. Temmyo, T. Takagahara, and H. Ando, "Exciton rabi oscillation in a single quantum dot," *Phys. Rev. Lett.*, vol. 87, no. 24, p. 246,401, Nov. 2001. doi: 10.1103/PhysRevLett.87.246401.

[3] H. Htoon, T. Takagahara, D. Kulik, O. Baklenov, A. L. Holmes, and C. K. Shih, "Interplay of rabi oscillations and quantum interference in semiconductor quantum dots," *Phys. Rev. Lett.*, vol. 88, no. 8, p. 087401, Feb. 2002. doi: 10.1103/PhysRevLett.88.087401.

[4] K. Asakura et al., "Excitonic rabi oscillations in self-assembled quantum dots in the presence of a local field effect," *Phys. Rev. B*, vol. 87, no. 24, p. 241,301, June 2013. doi: 10.1103/PhysRevB.87.241301.

[5] G. Y. Slepyan, S. A. Maksimenko, A. Hoffmann, and D. Bimberg, "Quantum optics of a quantum dot: Local-field effects," *Phys. Rev. A*, vol. 66, no. 6, p. 063804, Dec. 2002. doi: 10.1103/PhysRevA.66.063804.

[6] G. Y. Slepyan, A. Magyarov, S. A. Maksimenko, A. Hoffmann, and D. Bimberg, "Rabi oscillations in a semiconductor quantum dot: Influence of local fields," *Phys. Rev. B*, vol. 70, no. 4, p. 045320, July 2004. doi: 10.1103/PhysRevB.70.045320.

[7] M. Gross and S. Haroche, "Superradiance: An essay on the theory of collective spontaneous emission," *Phys. Rep.*, vol. 93, no. 5, pp. 301–396, 1982. doi: 10.1016/0370-1573(82)90102-8.

[8] N. E. Rehler and J. H. Eberly, "Superradiance," *Phys. Rev. A*, vol. 3, no. 5, pp. 1735–1751, May 1971. doi: 10.1103/PhysRevA.3.1735.

[9] J. C. MacGillivray and M. S. Feld, "Theory of superradiance in an extended, optically thick medium," *Phys. Rev. A*, vol. 14, no. 3, pp. 1169–1189, Sept. 1976. doi: 10.1103/PhysRevA.14.1169.

[10] C. R. Stroud, J. H. Eberly, W. L. Lama, and L. Mandel, "Superradiant effects in systems of two-level atoms," *Phys. Rev. A*, vol. 5, no. 3, pp. 1094–1104, Mar. 1972. doi: 10.1103/PhysRevA.5.1094.

[11] C. Vanneste and P. Sebbah, "Selective excitation of localized modes in active random media," *Phys. Rev. Lett.*, vol. 87, no. 18, p. 183,903, Oct. 2001. doi: 10.1103/PhysRevLett.87.183903.

[12] A. Fratalocchi, C. Conti, and G. Ruocco, "Mode competitions and dynamical frequency pulling in Mie nanolasers: 3d ab-initio Maxwell-Bloch computations," *Opt. Express*, vol. 16, no. 12, pp. 8342–8349, 2008. doi: 10.1364/OE.16.008342.

[13] B. Shanker, A. A. Ergin, K. Aygn¨, and E. Michielssen, "Analysis of transient electromagnetic scattering phenomena using a two-level lane wave time domain algorithm," *IEEE Trans. Antennas Propag.*, vol. 48, no. 4, pp. 510–523, 2000. doi: 10.1109/8.843664.

[14] B. Shanker, A. Ergin, M. Lu, and E. Michielssen, "Fast analysis of transient electromagnetic scattering phenomena using the multilevel plane wave time domain algorithm," *IEEE Trans. Antennas Propag.*, vol. 51, no. 3, pp. 628–641, Mar. 2003. doi: 10.1109/TAP.2003.809054.

[15] A. E. Yilmaz, J.-M. Jin, and E. Michielssen, "Time domain adaptive integral method for surface integral equations," *IEEE Trans. Antennas Propag.*, vol. 52, no. 10, pp. 2692–2708, Oct. 2004. doi: 10.1109/TAP.2004.834399.

[16] C. Glosser, B. Shanker, and C. Piermarocchi, "Collective rabi dynamics of electromagnetically coupled quantum-dot ensembles," *Phys. Rev. A*, vol. 96, no. 3, p. 033816, Sept. 2017. doi: 10.1103/PhysRevA.96.033816.

[17] C. Glosser, E. Lu, T. Bertus, C. Piermarocchi, and B. Shanker, "Acceleration techniques for semiclassical Maxwell–Bloch systems: An application to discrete quantum dot ensembles," *Comput. Phys. Commun.*, vol. 258, p. 107500, Jan. 2021. doi: 10.1016/j.cpc.2020.107500.

[18] C. Stroud and E. Jaynes, "Long-term solutions in semiclassical radiation theory," *Phys. Rev. A*, vol. 1, no. 1, pp. 106–121, Jan. 1970. doi: 10.1103/PhysRevA.1.106.

[19] C. Glosser, "The quest for active media models: A self-consistent framework for simulating wave propagation in nonlinear systems," Ph.D. dissertation, Michigan State Univ., East Lansing, 2018.

[20] L. Allen and J. Eberly, *Optical Resonance and Two-Level Atoms*. New York: Wiley, 1975.

[21] E. Lu, C. Piermarocchi, and B. Shanker, "Modeling radiation reaction induced superradiance in quantum dot systems." in *Proc. IEEE Int. Symp. Antennas Propag.*, July 2020, pp. 1653–1654. doi: 10.1109/IEEECONF35879.2020.9330119.

[22] A. Glaser and V. Rokhlin, "A new class of highly accurate solvers for ordinary differential equations," *J. Sci. Comput.*, vol. 38, no. 3, pp. 368–399, 2009. doi: 10.1007/s10915-008-9245-1.

[23] G. Rainò, M. A. Becker, M. I. Bodnarchuk, R. F. Mahrt, M. V. Kovalenko, and T. Stöferle, "Superfluorescence from lead halide perovskite quantum dot superlattices," *Nature*, vol. 563, no. 7733, pp. 671–675, 2018. doi: 10.1038/s41586-018-0683-0.

[24] T. Laske, H. Winter, and A. Hemmerich, "Pulse delay time statistics in a superradiant laser with calcium atoms," *Phys. Rev. Lett.*, vol. 123, no. 10, pp. 1–4, Sept. 2019. doi: 10.1103/PhysRevLett.123.103601.

[25] Y. Hua, "Estimating two-dimensional frequencies by matrix enhancement and matrix pencil," *IEEE Trans. Signal Process.*, vol. 40, no. 9, pp. 2267–2280, Sept. 1992. doi: 10.1109/78.157226.

[26] V. Jandhyala, E. Michielssen, and R. Mittra, "On the performance of different AR methods in the spectral estimation of FDTD waveforms," *Microw. Opt. Technol. Lett.*, vol. 7, 15, pp. 690–692, Oct. 1994. doi: 10.1002/mop.4650071504.